The impact of African aridity on the isotopic signature of Atlantic deep waters across the Middle Pleistocene Transition

Bruno Malaizé [a,*], Elsa Jullien [a], Amandine Tisserand [a,b], Charlotte Skonieczny [c], E. Francis Grousset [a], Frédérique Eynaud [a], Catherine Kissel [d], Jérôme Bonnin [a], Svenja Karstens [b], Philippe Martinez [a], Aloys Bory [c], Vivianne Bout-Roumazeilles [c], Thibaut Caley [a], Xavier Crosta [a], Karine Charlier [a], Linda Rossignol [a], José-Abel Flores [e], Ralph Schneider [f]

[a] UMR CNRS 5805 EPOC, Université Bordeaux I, 33405 Talence, France
[b] Department of Earth sciences, University of Bergen, Realfagb, Allègt. 41, Bergen, Bjerknes Centre for Climate Research, BCCR, Allègaten 55, 5007 Bergen, Norway
[c] FRE CNRS 3298 GEOSYSTEMES, Université de Lille I, 59655 Villeneuve d'Ascq, France
[d] Laboratoire des Sciences du Climat et de l'Environnement/IPSL, CEA/CNRS/UVSQ, Avenue de la Terrasse, Bat 12, 91198 Gif-sur-Yvette Cedex, France
[e] Departamento de Geología, Universidad de Salamanca, 37008, Salamanca, Spain
[f] Institut fuer Geowissenschaften, Christian-Albrechts-Universitaet, 10/24118 Kiel, Germany

ARTICLE INFO

ABSTRACT

A high resolution analysis of benthic foraminifera as well as of aeolian terrigenous proxies extracted from a 37 m-long marine core located off the Mauritanian margin spanning the last ~1.2 Ma, documents the possible link between major continental environmental changes with a shift in the isotopic signature of deep waters around 1.0–0.9 Ma, within the so-called Mid-Pleistocene Transition (MPT) time period. The increase in the oxygen isotopic composition of deep waters, as seen through the benthic foraminifera $\delta^{18}O$ values, is consistent with the growth of larger ice sheets known to have occurred during this transition. Deep-water mass $\delta^{13}C$ changes, also estimated from benthic foraminifera, show a strong depletion for the same time interval. This drastic change in $\delta^{13}C$ values is concomitant with a worldwide 0.3‰ decrease observed in the major deep oceanic waters for the MPT time period. The phase relationship between aeolian terrigeneous signal increase and this $\delta^{13}C$ decrease in our record, as well as in other paleorecords, supports the hypothesis of a global aridification amongst others processes to explain the deep-water masses isotopic signature changes during the MPT. In any case, the isotopic shifts imply major changes in the end-member $\delta^{18}O$ and $\delta^{13}C$ values of deep waters.

Introduction

During the Mid-Pleistocene Transition (MPT), which extends from 1.25 to 0.7 Ma (Clark et al., 2006, approximately centered around 0.9 Ma), drastic changes were observed in the glacial isotopic composition of deep-water masses of the Equatorial Atlantic Ocean (enriched $\delta^{18}O$ values and depleted $\delta^{13}C$ values) (Flower et al., 2000; Schefuß et al., 2003; Raymo et al., 2004). Similar shifts in isotopic values (i.e., enriched $\delta^{18}O$ values and depleted $\delta^{13}C$ values) were observed in cores from different oceanic basins, highlighting the global aspect of such changes (Raymo et al., 1997; deMenocal, 2004; Ravelo et al., 2004; Lisiecki and Raymo, 2005; Hoogakker et al., 2006). Global trends are only apparent in deep-water signatures. Conversely, records of surface conditions vary: cooling is shown in the equatorial Atlantic (Marlow et al., 2000), while stable sea-surface temperatures are

observed in the tropical Pacific warm pool (deGaridel-Thoron et al., 2005) at the same time. The global $\delta^{18}O_{benthic}$ enrichment mainly results from the build up of large continental ice sheets at high latitudes. The decrease in $\delta^{13}C_{benthic}$ values (>0.3‰) between 1.1 and 0.9 Ma has been attributed to a net addition of a ^{12}C-enriched reservoir into the ocean (Raymo et al., 1997). Two main candidates were proposed: (1) marine organic matter exposed on continental shelves as sea level dropped, or (2) carbon input from the terrestrial biosphere reservoir. The first hypothesis suggests an increase in the mean ocean nutrient content, implying changes in the Atlantic-Pacific oceanic $\delta^{13}C$ gradient. As no such changes are observed in the inter-basin $\delta^{13}C$ gradient nor in the Redfield nutrients, the first hypothesis has been disregarded. This left the second hypothesis, suggesting, without other robust arguments, a global increase in aridity after 0.9 Ma (Raymo et al., 1997). A global carbon isotope budget, applied to glacial–interglacial climatic shifts (Maslin and Thomas, 2003), estimated the effect of different parameters such as terrestrial biomass volume and carbon isotopic changes (C_3/C_4), together with changes due to exchange of gas hydrates. This study proposed an average shift

* Corresponding author at: University Bordeaux1, UMR 5805 EPOC, France. Fax: +33 5 56 84 08 48.
E-mail address: b.malaize@epoc.u-bordeaux1.fr (B. Malaizé).

in the global oceanic $\delta^{13}C$ values of about 0.3‰ between the last glacial maximum (LGM) and the Holocene, reappraising previous average estimates of ~0.4‰ (Curry et al., 1988; Duplessy et al., 1988). Maslin and Thomas (2003) highlighted here the important consequence of bigger ice sheets on the receding of terrestrial biomass and the impact on the global carbon isotope budget. For the MPT, global models (e.g., Hoogakker et al., 2006) have suggested that such oceanic $\delta^{13}C$ fluctuations could result from concomitant changes in the burial fluxes of organic and inorganic carbon. On the Atlantic coast of Africa, previous studies on marine records, focusing on the MPT, revealed environmental changes over the continent, linked to atmospheric changes, bringing new pieces of evidence for aridification (Dupont et al., 2001; Schefuß et al., 2003) and wind intensification (Marlow et al., 2000). DeMenocal has even suggested that such changes could have influenced African hominid evolution (deMenocal, 2004).

In addition to this peculiar isotopic shift occurring during the MPT, isotopic changes are observed in Equatorial Atlantic deep-water masses on orbital time scales (Duplessy et al., 1980; Duplessy and Shackleton, 1985; Curry et al., 1988; Oppo and Lehman, 1993; Raymo et al., 1997; Flower et al., 2000; Curry and Oppo, 2005). In the modern Atlantic Ocean and more generally during interglacial periods, the northward-flowing surface water becomes denser and sinks as the southward-flowing North Atlantic Deep Water (NADW). This deep-water mass is characterized by rather $\delta^{18}O$ values (~3‰) due to reduced continental ice sheet volume, and by high $\delta^{13}C$ values (>1‰) resulting from young waters sinking from the surface, after marine productivity has removed nutrients (PO_3, NO_3) and ^{12}C,

enriching it in ^{13}C (Broecker and Peng, 1982; Curry et al., 1988). This carbon isotopic signature can be traced as far south as the equatorial region, at depths of about 2500–3000 mbs (Flower et al., 2000) (Fig. 1). The southern part of the deep Atlantic Ocean hosts Lower Circumpolar Deep Water (LCDW), originating from the Southern Ocean. This water mass is characterized by lower $\delta^{13}C$ values (between 0.5 and 0‰, after Kroopnick, 1985). Because these southern deep waters have been isolated from the surface for a long time, the continuous oxidation of low-$\delta^{13}C$ organic matter at depth has lowered its $\delta^{13}C$ value.

During a glacial period, the build-up of huge continental ice sheets influences the dynamics of this deep-water circulation, reducing NADW formation, and delivering it to shallower depths, generating the Upper North Atlantic Deep Water (UNADW). Such change in the deep circulation allows a stronger intrusion of South Oceanic Waters (SOW) at northern latitudes (Fig. 1), for which the aging effect has shifted their carbon isotopic composition to negative values. The mixing between these water masses (SOW and UNADW) led to lower $\delta^{13}C$ values at equatorial latitudes (Duplessy et al., 1988; Sarnthein et al., 1994; Flower et al., 2000).

A schematic pattern of changes in the Atlantic deep-water masses circulation can even be drawn by using their isotopic compositions, as the result of mixing between two end-members, with high $\delta^{13}C$ (>0.5‰) and low $\delta^{18}O$ (around 2.5‰) values, attributed to interglacial North Atlantic Deep Waters (NADW), and lower $\delta^{13}C$ (<0.5‰) and higher $\delta^{18}O$ (~4.5‰), attributed to glacial South Oceanic Waters (SOW) (Duplessy and Shackleton, 1985; Curry et al., 1988; Sarnthein
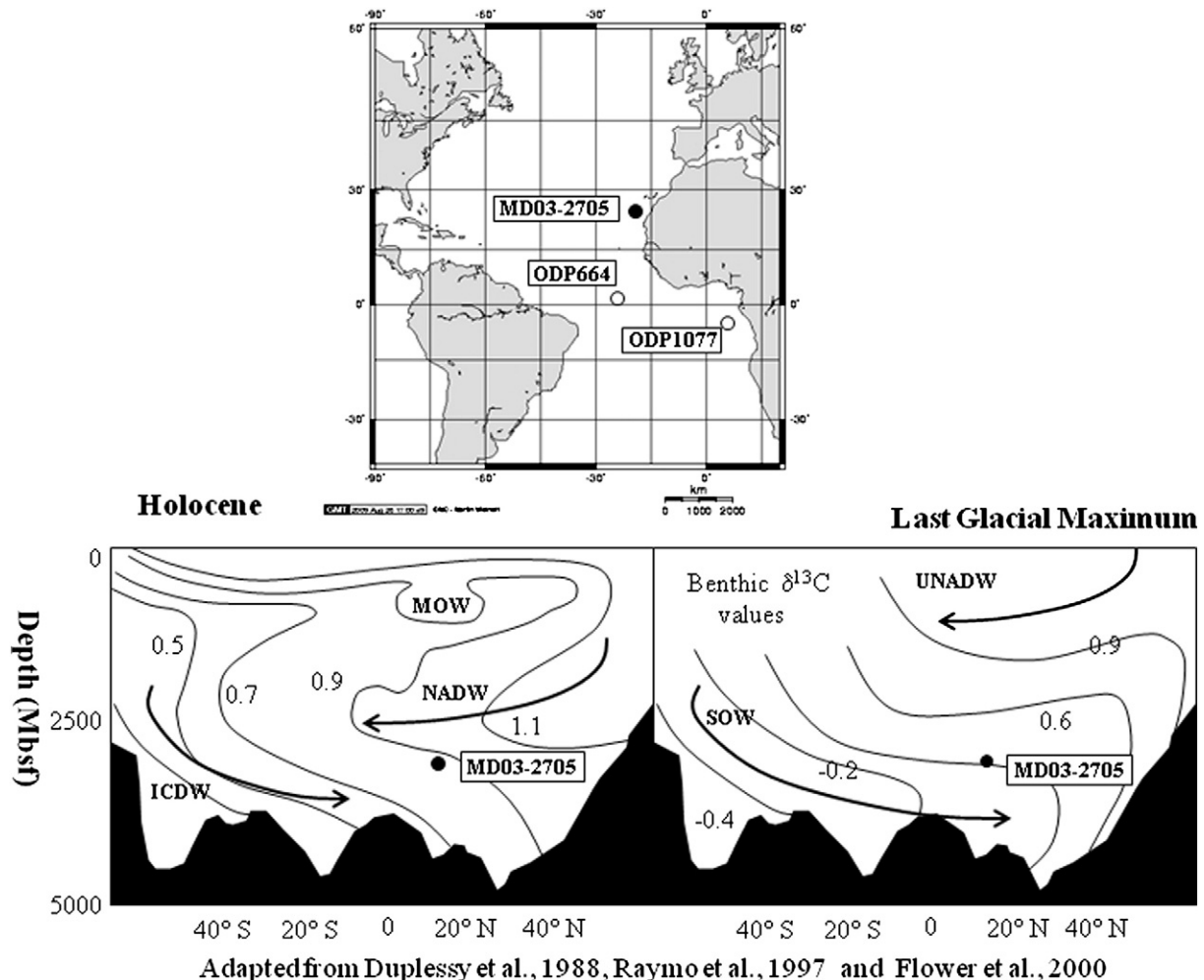
Figure 1. Cross sectional maps of the Atlantic ocean. Location of cores MD03-2705 (this study), ODP 664 (Raymo et al., 1997) and ODP1077 (Dupont et al., 2001; Schefuß et al., 2003) and carbon isotopic values ($\delta^{13}C$) of water masses.

et al., 1994; Flower et al., 2000; Curry and Oppo, 2005) (Fig. 1). Such isotopic oscillations have been observed over tens to hundreds of thousands year time scales (Raymo et al., 1997), but also for millennial-scale events over the last climatic cycle, shifting from warm to cold climatic conditions, associated to abrupt NADW circulation changes (e.g., Vidal et al., 1999; Shackleton et al., 2000).

As described previously, glacial–interglacial variations of global oceanic $\delta^{13}C$ values could also record the expansion and contraction of the terrestrial biosphere (Maslin and Thomas, 2003). However, the consequence of such an effect might have been inadequate for the MPT time period. Indeed, for the LGM–Holocene transition, a 1‰ change in the global $\delta^{18}Osw$ value has been accompanied by a 0.3‰ change in the global $\delta^{13}C$ value. Since the $\delta^{18}O$ difference between successive glacial across the MPT time interval is considerably smaller than across the last deglaciation, it seems fair to assume that the additional carbon input from the larger ice sheets was also smaller than 0.3‰. This hypothesis is thus not sufficient to explain the entire decrease in benthic $\delta^{13}C$ values observed for successive glacial periods across the MPT.

In order to investigate these deep-water isotopic composition changes and to distinguish the shorter-term fluctuations (e.g. glacial–interglacial deep oceanic circulation changes) from the MPT shift (possibly linked with atmospheric circulation changes), we present here a study of a deep marine core from the tropical Atlantic Ocean, covering the past 1.10 Ma. Isotopic analyses of stable isotopes ($\delta^{18}O$ and $\delta^{13}C$) were made on benthic foraminifera to characterize variations in the isotopic composition of deep-water masses. The core is located along the north western African margin and heavily influenced by atmospheric dust plumes from the Sahara desert. This allows us to study aridity changes over the African continent in parallel with the stable isotope shifts and therefore to test the global aridity hypothesis.

Setting and methods

Core MD03-2705 is located in the eastern tropical Atlantic Ocean [18°05.81′N; 21°09.19′W; 3085 meters below sea floor (mbsf)]. The area is sensitive enough to record the balance between the NADW and the SOW water masses (Fig. 1). Previous estimates of mean accumulation rate of about 3.4 cm/ka (Jullien et al., 2007; Tisserand et al., 2009) date the oldest part of this 37-m-long core at greater than 1 million years. The core was retrieved from a bathymetric dome, 300 m above the surrounding seafloor, thus preventing possible perturbations of the sediment from gravity and bottom currents (Jullien et al., 2007).

Benthic foraminifera have been handpicked under stereomicroscope from dry sediment sieved at 150 μm. The sampling interval was 10 cm and splitting of the dry samples was done when weight exceeded 0.5 g. A maximum of 4 splits were made for sample at 1.022 Ma (1.8 g). Total amount of picked individuals per sample ranges from 81 at 0.910 Ma to 521 at 0.968 Ma (mean 218). The number of counted specimens per sample has been normalised to sample weight. Data presented in this study are limited to those of the Benthic Foraminiferal Number (BFN) that shows the total number of individuals per gram of dry sediment and Uvigerina peregrina abundance changes which are considered as an indicator of surface productivity (Lutze and Coulbourn, 1984, Loubere, 1991).

Isotopic analyses were made on monospecific samples of the bathyal epifaunal species of benthic foraminifera Planulina wuellerstorfi, and are therefore suitable to record variations in the deep-water isotopic composition. For each sample, 2 to 3 individuals were picked and dissolved in acid via the Micromass Multiprep autosampler system. The resulting carbon dioxide gas was subsequently analysed against the international reference standard NBS 19, using an Optima Micromass mass spectrometer. Measurements were carried out at the Bordeaux 1 University, within the EPOC isotopic laboratory. Triplicate measurements were made for each depth horizon (1 cm)

to reduce uncertainties. The analytical precision is better than 0.05‰ for $\delta^{18}O$ and 0.03‰ for $\delta^{13}C$. A +0.64 mil^{-1} correction factor was applied to Planulina wuellerstorfi $\delta^{18}O$ values, according to previous calibration studies (Shackleton and Opdyke, 1973; Duplessy et al., 1984). No correction is necessary for Planulina wuellerstorfi $\delta^{13}C$ values.

Major elements were measured in the bulk sediment using the Bremen XRF-Cortex facility, with a 1-cm step resolution (Jullien et al., 2007). Here, we focus on the titanium (Ti) record as a tracer of terrigenous supply (Richter et al., 2006) derived from preferential aeolian contributions (Itambi et al., 2009). The percentage of calcium carbonate is based on the Ca record, using a previously established calibration (Tisserand et al., 2009), that links XRF-based Ca measurements with the classical volumetric method using Bernard calcimeter (Huelsemann, 1966; Muller and Gatsner, 1971). Biogenic opal is a minor to negligible component of the sediment (less than 10%) in this area (deMenocal et al., 2000). A first-order approximation of the dust content is obtained by assuming that the non-carbonate fraction represents the dust fraction as proposed by Jullien et al. (2007) and Tisserand et al. (2009), as well as by deMenocal et al. (2000) for the neighboring marine core ODP-658.

According to this hypothesis, and in a first-step approach, the concentration of terrigenous particles is estimated using the following relationship:

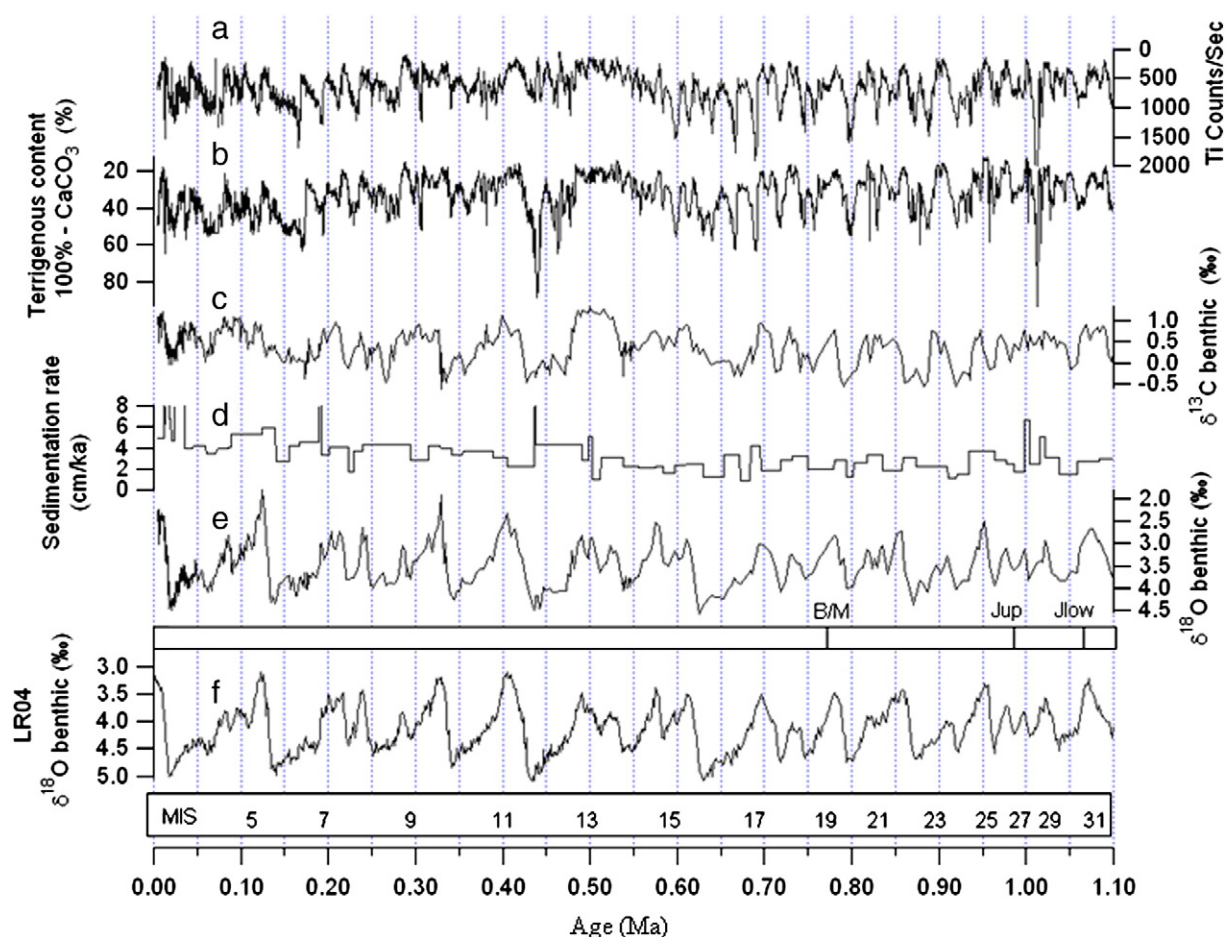Terrigenous content (%) = 100−CaCO$_3$ content

Semi-quantitative quartz content estimates in the clay–mineral fraction have been carried out using X-ray diffraction at the University of Lille. Samples were prepared following the protocol of Bout-Roumazeilles et al. (1999). X-ray diagrams were obtained using a BRUKER D4 Endeavor in association with the Lynxeye fast detector (Cu X-ray tube; 35 kV voltage; 30 mA intensity). XRD runs were performed routinely for each sample between 2.49 and 32.49°2θ) on air-dried samples. Quartz intensity (in counts per second) was measured on the 4.26 Å peak using the Macintosh MacDiff® 4.2.5 software (Petschick, 2000).

For paleomagnetic analyses, u-channels were sampled in the deepest part of the core, between 27 mbsf and 29.5 mbsf and below 33 mbsf. The analysis of the natural remanent magnetization (NRM) was conducted using a 755-R 2G-cryogenic magnetometer equipped with high-resolution pick-up coils within the μ-metal shielded room of LSCE (Weeks et al., 1993). Stepwise alternating field demagnetization was conducted with 13 successive steps from 0 to 80 mT. The direction of the characteristic remanent magnetization and the mean angular deviation (MAD) were determined using a PCA analyses (Kirschvink, 1980; Mazaud, 2005).

Stratigraphy of the upper part of core MD03-2705, covering the last two climatic cycles, has been published in Jullien et al. (2007) and in Tisserand et al. (2009). A new stratigraphy, based on a fifth-order polynomial regression, is proposed for the past 0.22 Ma (Matsuzaki et al., 2011). Stratigraphy of the lower part of the core was developed by tuning the $\delta^{18}O$ benthic record to the LR04 reference record (Lisiecki and Raymo, 2005), using the Analyserie program (Paillard et al., 1996) (Fig. 2). The $\delta^{18}O$ benthic record in core MD03-2705 is offset by a relatively constant value of −0.5‰ relative to the LR04 record. The constancy of this difference is remarkable, given that Lisiecki and Raymo (2005) used multiple benthic records from different cores to build their stack, while MD03-2705 $\delta^{18}O$ curve originates from a single core.

Stratigraphy of the lower part of core MD03-2705 is further constrained using the paleomagnetic record. Three main polarity reversals are identified with a MAD value very rarely exceeding 7–8° (maximum value: 16°): a reverse to normal polarity centered around 35.85 mbsf, a normal to reverse polarity around 33.60 mbsf and a reverse to normal polarity at 28.30 mbsf. These three polarity reversals correspond to the lower and upper Jaramillo and to the

Figure 2. (a) Ti qualitative content (XRF) in core MD03-2705; (b) Terrigenous content approximation in core MD03-2705; (c) Benthic δ^{13}C record in core MD03-2705; (d) sedimentation rate in core MD03-2705; (e) Benthic δ^{18}O record in core MD03-2705. (f) Benthic δ^{18}O record from LR04 stack (Lisiecki and Raymo, 2005). Main paleomagnetic horizons are marked (B/M: Bruhnes-Matuyama, Jup: upper Jaramillo, Jlow: lower Jaramillo).

Matuyama/Bruhnes reversals. They occur during Marine Isotopic Stages (MIS) 31, 27 and 19 respectively, consistent with previous studies (Shackleton et al., 1990; Horng et al., 2002). The ages assigned to these horizons in core MD03-2705, when reported on the LR04 scale (1.07 Ma, 0.988 and 0.781 Ma, respectively, for 35.85, 33.6 and 28.3 mbsf) (Horng et al., 2002), are consistent within about 5 ka uncertainty with the radiometric ages of the reversals at 1.053 ± 6 Ma, 0.986 ± 5 Ma and 0.779 ± 2 Ma (Singer et al., 1999 and references therein, Singer and Brown, 2002). All of the chrono-stratigraphic information for this core is internally consistent.

Unfortunately, the oldest sample extracted from core MD03-2705 (1.1 Ma) is not old enough to cover the whole MPT time interval, starting around 1.25 Ma according to Clark et al. (2006). Our record is therefore missing the background variations that lead up to this transition, and might possibly miss some events which could had have higher amplitude than the ones discussed in this work. Meanwhile, the largest changes recorded during the MPT are usually centered around 0.9 Ma, well within our record.

Results

Continental aridity proxies

The carbonate-free fraction of the core is a mixture of clay minerals and fine silt-sized quartz brought by the winds, along with rare freshwater diatoms and phytoliths. Because of low amounts of biogenic opal in the sediment, the aeolian dust fraction was estimated by difference between the total and the CaCO$_3$ fraction (see setting and method section). This approximation is supported by the XRF measurements of terrigenous elements such as Ti in the bulk sediment, which show a very good correlation with the percentage of the terrigenous fraction (Fig. 2).

The terrigenous percentages may not solely reflect changes in dust inputs as it is also dependant on CaCO$_3$ productivity and sedimentation, including possible dissolution effects. The carbonate microfossils (foraminifera), however, present no imprint of dissolution. Moreover, in a previous paper focusing on MIS 6, specific counts (on smear slides) of aeolian quartz particles in core MD03-2705, have clearly shown the link between aeolian inputs and terrigenous index (100% − CaCO$_3$) (Tisserand et al., 2009). Here, the good correlation between the aeolian terrigenous fraction and the quartz content estimates in the clay–mineral fraction during the MPT also supports the validity of the assumption that the percentage of mineral dust primarily reflects an intensification of the aeolian terrigenous supply, which can be interpreted in this particular sedimentary setting as variations in aridity (Rea, 1994), at least for this period.

Ti variations, together with the terrigenous particle concentrations and sedimentation rate variations are compared over the past 1.1 Ma in Figure 2. Some rapid increases of the sedimentation rate are found during glacial MIS 28, 12, 6 and 2 periods. During MIS 28 (around 1.025 Ma), the sharp increase is clearly linked to an exceptional volcanic event, marked by an ash layer. Both the amount of Ti and the terrigenous content records proxies record one of their

Table 1
Glacial and interglacial intervals, together with their mean isotopic values.

M.I.S.	Depth (cmbsf)	Age (cal.) ka B. P.	$\delta^{18}O$ mean value (‰)	$\delta^{13}C$ mean value (‰)
1	0 – 28	0 – 10.07	2.480	0.961
2	104 – 160	18.045 – 21.142	4.266	0.247
3	218 – 346	25.897 – 47.693	3.767	0.684
4	385 – 410	56.917 – 63.134	3.929	0.229
5	450 – 720	73.215 – 128.977	2.984	0.747
6	750 – 790	134.762 – 141.836	4.256	0.336
7	1000 – 1220	185.430 – 240.973	3.032	0.563
8	1250 – 1350	247.711 – 274.666	3.868	0.106
9	1380 – 1550	283.166 – 329.560	2.929	0.531
10	1580 – 1670	337.000 – 362.077	4.002	− 0.04
11	1800 – 1860	398.600 – 422.714	2.799	0.767
12	1900 – 2080	437.000 – 477.134	4.085	− 0.052
13	2100 – 2251	481.782 – 532.933	3.205	1.079
14	2271 – 2310	538.450 – 556.000	3.871	0.329
15	2350 – 2440	575.000 – 618.000	3.132	0.627
16	2460 – 2480	626.000 – 638.000	4.375	0.161
17	2570 – 2650	684.000 – 712.500	3.301	0.459
18	2660 – 2770	718.000 – 755.000	3.819	0.131
19	2790 – 2850	765.000 – 790.500	3.139	0.203
20	2860 – 2880	794.000 – 805.902	3.885	− 0.262
21	2911 – 3011	818.000 – 858.000	3.033	0.414
22	3041 – 3091	867.600 – 887.671	4.088	− 0.349
23	3121 – 3140	901.341 – 910.000	3.473	0.326
24	3161 – 3181	927.000 – 936.000	3.752	− 0.292
25	3221 – 3261	944.000 – 952.000	2.824	0.530
26	3271 – 3301	958.000 – 971.000	3.633	0.243
27	3321 – 3381	978.000 – 1001.000	3.344	0.419
28	3391 – 3421	1002.500 – 1012.000	3.659	0.456
29	3451 – 3471	1020.000 – 1025.200	3.081	0.717
30	3491 – 3541	1031.600 – 1058.000	3.736	0.290
31	3561 – 3621	1065.429 – 1087.500	2.883	0.769
32	3641 – 3661	1094.500 – 1101.333	3.582	0.232
33	3671 – 3681	1104.666 – 1108.000	3.046	0.822

highest values within the ash layer (Fig. 2). Otherwise, variations in the sedimentation rates are rather low and steady. A strong similarity between the terrigenous proxies and $\delta^{13}C_{benthic}$ curve is clear for the earliest part of the record, from 1.1 Ma to 0.7 ka while discrepancies appear for the latest part, from 700 ka to present day (Fig. 2). Within the MPT transition, between 1 Ma and 0.9 Ma, glacial periods (from MIS 26 to MIS 22) are characterized by a progressive increase in both terrigenous proxies. Variability decreases in both records to a plateau within MIS 15 and MIS 13, i.e. between 0.60–0.45 Ma.

Deep-water masses isotopic signature

We defined time intervals corresponding to full glacial and interglacial periods for the last 1.1 Ma in order to identify the two primary end-member water masses (i.e., similar to NADW and SOW). Climatic transitions (i.e., terminations/deglaciations), during which the water masses mixing readjustment occurs, have been removed in this operation. The selected time periods, and the corresponding depth intervals, are presented in Table 1.

An X-Y plot of $\delta^{18}O$ values and $\delta^{13}C$ values provides a clear graphical separation of interglacial and glacial periods (Fig. 3). Interglacial periods, concentrated on the upper part of the graph, are characterized by low $\delta^{18}O$ and high $\delta^{13}C$ values, while glacial periods, on the lower part of the graph, are identified by high $\delta^{18}O$ and low $\delta^{13}C$ values. Interglacial values are scattered around the NADW reference value, in agreement with the modern hydrology off the Mauritanian margin. Glacial periods conversely show a scattering around the SOW reference value.

For the glacial values of this scatter plot, some isotopic differences can be observed through time, defined as clusters (Fig. 3) in the following description. For oldest glacials, i.e. from MIS 32 to 28, isotopic values are in between the two end-member values (Fig. 3). The low amplitude $\delta^{18}O$ and $\delta^{13}C$ variations characterizing MIS 32 to 28 suggest

rather small glacial-interglacial deep-water masses variations (Fig. 2). The MPT (from cluster MIS 28–32 to cluster MIS24–20 in Fig. 3) is marked by a clear shift in range of $\delta^{13}C$ values with lower values during both glacial and interglacial periods compared to the previous intervals, while the total amplitude of the $\delta^{18}O$ signal is only slightly enriched. The most recent period, from MIS 16 to 2, shows a shift back toward higher $\delta^{13}C$ values for both glacial and interglacial periods. Only MIS 12, within this recent period, experiences $\delta^{18}O$ and $\delta^{13}C$ isotopic values comparable to those found within MIS 32 to MIS 28 (Fig. 2). This explains the overlap between these last two clusters (on the X–Y plot, Fig. 3). The $\delta^{13}C$ signal thus displays a peculiar temporary feature over the MPT interval (from cluster MIS 28–32 to cluster MIS 24–20), with both glacial and interglacial-depleted values (Figs. 2 and 3). Contrastingly, the glacial $\delta^{18}O$-values increased during the MPT and progressively reached the recent glacial signature (MIS 16 to 2). Meanwhile the interglacial $\delta^{18}O$ values remained rather stable (even slightly decreasing) over the MPT interval compared to the increase observed on the more recent periods (MIS 16 to 2), when the $\delta^{18}O$ amplitude reached its maximum actual range.

Discussion

Continental-deep ocean linkage on the African margin

For the deep-water carbon isotopic composition, a marked depletion is observed in core MD03-2705 between 1.10 and 0.80 Ma, with the lowest $\delta^{13}C$ values reached during MIS 24, 22 and 20 (Fig. 2). This drop in the deep marine $\delta^{13}C$ values is in complete agreement (in both timing and amplitude) with what was observed in the nearby marine core ODP664 (Raymo et al., 1997).

In marine record MD03-2705, a strong similarity in shape between the terrigenous content and $\delta^{13}C$ benthic curve can be observed for the earliest part of the record, from 1.1 Ma to 700 ka,
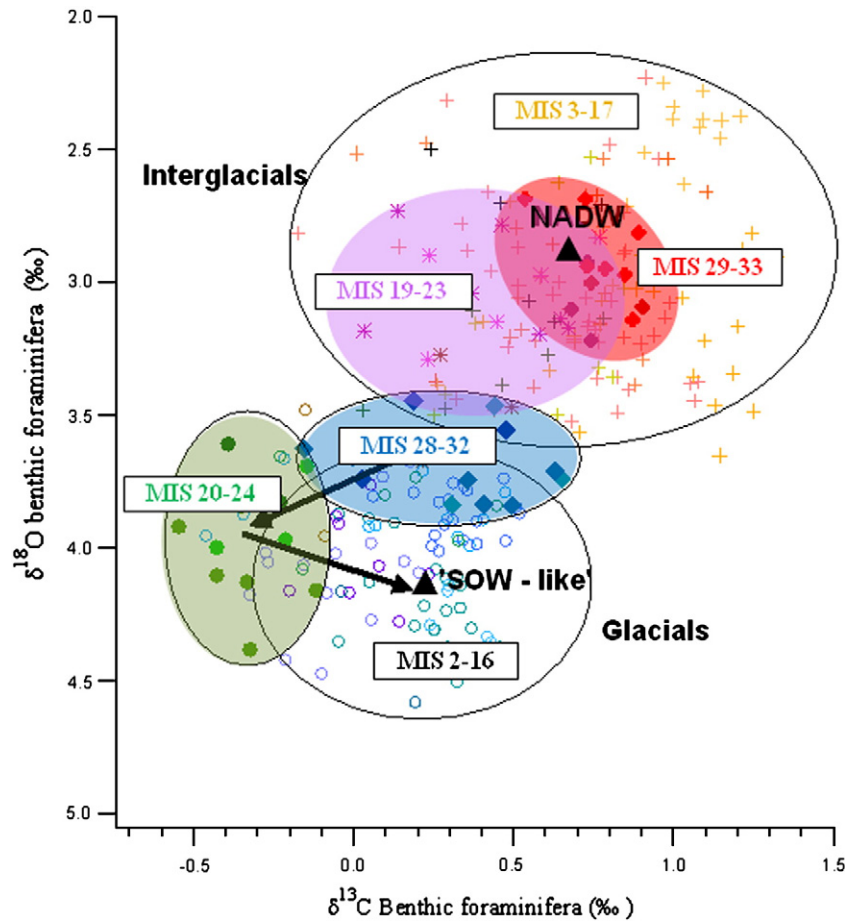
Figure 3. Isotopic composition of deep-water masses. Crosses and stars (red and pink) represent interglacial periods. Diamonds and circles (blue and green) represent glacial periods. We have distinguished between recent glacial periods, from MIS 2–16 (clear blue circles), oldest glacial periods (blue diamonds: MIS 28–32, and plain green circles: MIS 20–24), as well as recent interglacial intervals, from MIS 3–17 (crosses) and oldest interglacials (red bold stars: MIS 29–33 and pink stars: MIS 19–23) as discussed in text. Black arrows represent evolution from older time periods to younger ones. Black triangles present the modern isotopic composition of NADW and of a southern water mass which isotopic composition could be associated to a 'SOW-like' end-member.
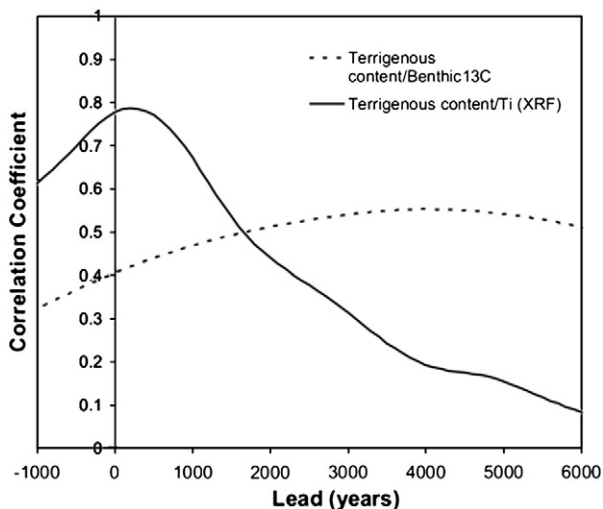
Figure 4. Correlation as a function of lag (years) for the interval 700-1100 kyrs between the terrigenous content and the benthic $\delta^{13}C$ records (dash line) and between the terrigenous content and Titanium (Ti) measurement with the XRF core scanner records (plain line). Maximum correlation (0.55) are achieved for a 4000-year lead of terrigenous content vs benthic $\delta^{13}C$. Maximum correlation (0.79) indicate a quasi-in phase relationship between terrigenous content and Titanium (Ti) measurement with the XRF core scanner.

while discrepancies appear for the latest part, from 700 ka to present day (Figs. 2 and 5). For the MPT time interval, between 1.0 and 0.7 Ma, the marked peaks in the $\delta^{13}C$ benthic record appear to be in phase with increases in the Ti content, the terrigenous percentage and semi-quantitative quartz content records (Fig. 6). Lag-correlation analysis (using MATLAB software) between the $\delta^{13}C$ benthic and terrigenous content records between 1.0 and 0.7 Ma reveals a maximum correlation of 0.55 for a 4000-yr lead of the terrigenous signal (Fig. 4). The relatively weak correlation suggests that, while a clear link exists between continental aridity and the $\delta^{13}C$ benthic signature, this link is probably not direct (West African terrigenous signal possibly leading global aridification) and that other processes are probably involved in the carbon isotopic changes of deep-water masses.

As shown by the $\delta^{18}O$ benthic record, the MPT corresponds to progressively colder glacial conditions, characterized by the building of larger continental ice sheets. As suggested by paleodata from the equatorial Atlantic Ocean (deMenocal, 1995; Jullien et al., 2007; Mulitza et al., 2008), as well as modelling results (Tjallingii et al., 2008; Kageyama et al., 2009), a strengthening of the atmospheric circulation cells, accompanied by a southward shift in the pattern of the Inter-Tropical Convergence Zone (ITCZ), is expected during these colder periods. The southward shift of the ITCZ would have extended the arid belt further south in Northwest Africa, and is likely to have increase wind stress, as observed during the last two climatic cycles (Jullien et al., 2007; Tisserand et al., 2009; Matsuzaki et al., 2011). Increasing values of dust content are consistent with these changes (Fig. 4). The hypothesis proposed by Raymo et al. (1997) seems to

be supported by our Mauritanian margin record. Indeed, an extension of the arid belt associated with stronger winds blowing westward over the African continent might have increased the input from a depleted ^{13}C carbon reservoir into the ocean, contributing to the general lower $\delta^{13}C$ benthic values.

A putative atmospheric circulation change during the MPT, associated with a southward shift in the migration pattern of the ITCZ, may have directly impacted the local oceanic environment, and thus the benthic $\delta^{13}C$ signature. Today, strong upwelling takes place on the Mauritanian margin, which affects surface $\delta^{13}C$ values of dissolved inorganic carbon via stronger productivity (Mackensen and Bickert, 1999). Although core MD03-2705 is not located directly within the upwelling cells, some filaments of upwelled nutrient-enriched waters could reach our site, during specific periods (Matsuzaki et al., 2011). In the context of sea-level falls during glacial periods, the geographic influence of upwelled waters, due to the westward Ekman deviation of the Canary Current, might have shifted offshore toward the outer shelf and upper slope (Bertrand et al., 1996), moving the productive areas off-shore as well (Martinez et al., 1996). In addition, stronger westward winds could have increased the strength of the upwelling, increasing the phytoplankton productivity. *U. peregrina* generally appears more abundant during glacial periods such as MIS 30, 28 and 26 when Ti content is also higher (Fig. 6). This is similar to what has been observed for the late quaternary in the South Atlantic Ocean by Schmiedl and Mackensen (1997). This increase in the amount of *U. peregrina* reflects higher oceanic productivity during MIS 30, 28 and 26 that could be associated with a more vigorous upwelling due to stronger winds blowing from the east. The later peak of *U. peregrina* (Fig. 6f) occurring during MIS 28 is most probably related to enhanced fertilization of surface water by volcanic ashes found during this interval (confirmed by magnetic susceptibility) rather than

upwelling intensity. Meanwhile, no clear changes are observed while entering into colder glacial periods within the MPT (e.g. MIS 24). The direct influence of lower sea level on the paleoproductivity at the MD 03-2705 core site is therefore uncertain. To further investigate the possible changes and transfer of the carbon isotopic signal from the surface to the deep water, future work should focus on the isotopic and elemental characterization of the thermocline layer. A $\delta^{13}C$ record of different planktonic foraminifera species of core MD03-2705 is required to test this hypothesis.

The contribution of the West African margin aridity alone would obviously be too small to affect the global signature of the whole oceanic deep waters. Meanwhile, other paleo-records help to extent such hypothesis to the rest of the African continent. For the Benguela basin (ODP 1084) along the south tropical Atlantic African coast, intensification of the upwelling cells has been observed during the MPT, and linked with the aridification of the African continent (Marlow et al., 2000). In the Angola basin (ODP 1075), vegetation changes of the African continent have been recorded as early as 1.05 Ma (Dupont et al., 2001). For a neighbouring core, a record of African C_4 plant abundance, derived from compound-specific carbon isotope analysis of wind-transported terrigenous plant waxes, confirms some changes in the atmospheric moisture content during the MPT (Fig. 6) (Schefuß et al., 2003). The abundance of C_4 plants, found predominantly in tropical savannahs and semi-deserts, seems to be directly linked with the sea surface temperature record and the atmospheric moisture content. The establishment and persistence of C_4 grassland around 0.9 Ma has been explained by a large-scale aridification of the African continent during this time period (Schefuß et al., 2003). Despite uncertainties linked to different age scales, increases in C_4 percentage in marine core ODP1077 in the Angola basin seem to be in phase with wind-strengthening proxies (Ti and Quartz counts) in
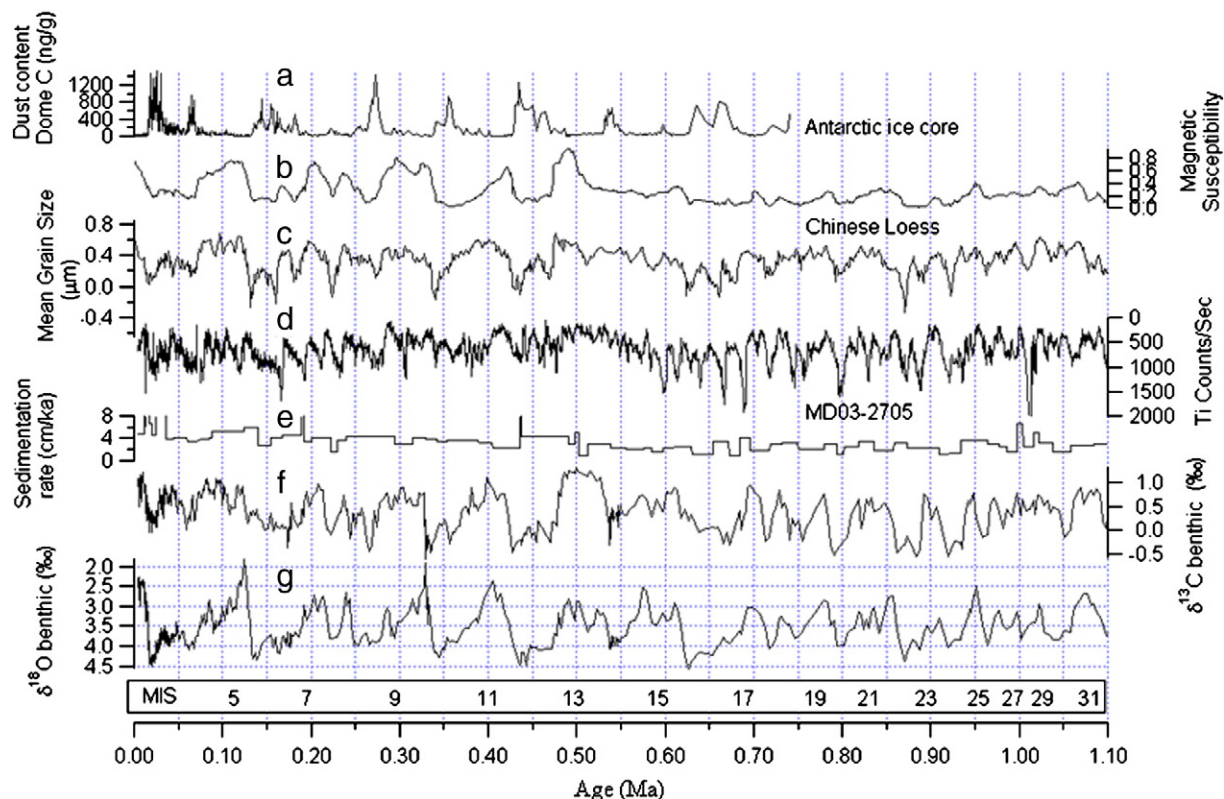
Figure 5. (a) Dust content in Dome C ice Core (Antarctica) (Epica community members, 2004); (b) Magnetic susceptibility of East Asian Loess (Summer monsoon proxy) (Sun et al., 2006); (c) Mean grain size composition of East Asian Loess (Winter monsoon proxy) (Sun et al., 2006); (d) Ti qualitative content in core MD03-2705 (aridity proxy); (e) Sedimentation rate in core MD03-2705; (f) $\delta^{13}C$ benthic record from core MD03-2705; (g) Benthic $\delta^{13}C$ record for core MD03-2705.
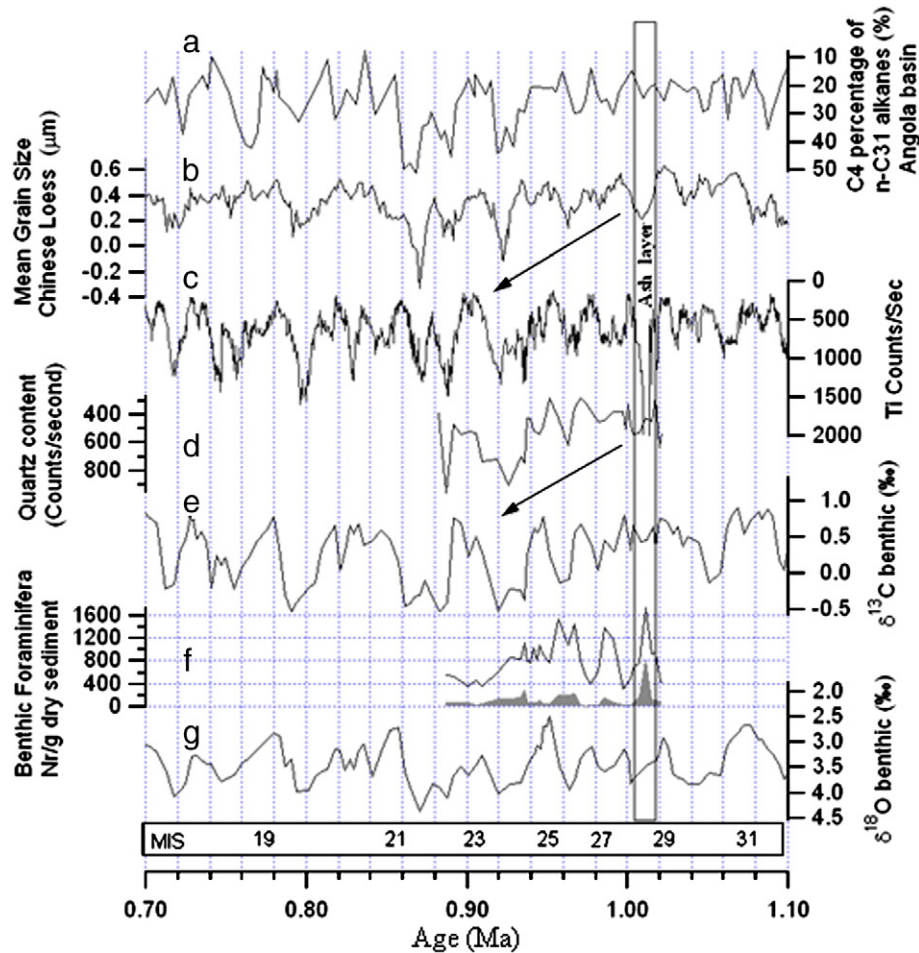
Figure 6. Zoom on the MPT:(a) C4 plant percentage of n-C31 alkanes (%) from the Angola basin (ODP 1077) (Schefuß et al., 2003)(b) Mean grain size composition of East Asian Loess (Winter monsoon proxy) (Sun et al., 2006)(c) Ti qualitative content in core MD03-2705 (aridity proxy);(d) Quartz content in core MD03-2705;(e) δ^{13}C benthic record from core MD03-2705;(f) Benthic foraminiferal analysis in core MD03-2705. BFN (black line) and *Uvigerina peregrina* (grey area), indicating higher paleoproductivity for high values.(g) Benthic δ^{18}O record for record core MD03-2705.The vertical grey band highlights the volcanic ash layer found in core MD03-2705.

core MD03-2705 off the Mauritanian margin (Fig. 6). The hypothesis of a southward shift of the ITCZ, leading to aridification and erosion of previously moist areas, is in agreement with the absence of any typical arid markers within the clay mineral association in our record. Indeed African arid sources provide fibrous clay minerals as palygorskite or sepiolite (Bout-Roumazeilles et al., 2007; Jullien et al., 2007) that are not particularly abundant over the MPT.

The carbon isotopic MPT depletion—a response to an increase in global aridity?

As discussed previously, an expansion of the mean global ice volume could have occurred for each successive glacial interval within the MPT time interval, dragging a perennial polar front southward. This latitudinal shift might have forced the southward migration of NADW convection centers, reducing the convection efficiency, as is observed for recent glacial periods. The subsequent change in the latitudinal distribution of deep-water masses would have impacted the δ^{13}C benthic record in core MD03-2705, assuming that the deep-water masses are characterized by a unique isotopic signature (high δ^{13}C and low δ^{18}O for NADW, and low δ^{13}C and high δ^{18}O for SOW). The reduction of NADW formation during each successive glacial interval within the MPT might have allowed the northward penetration of the SOW from 1.0 to 0.8 Ma, producing noticeable δ^{13}C depletion, along with a δ^{18}O enrichment in the MD03-2705 benthic isotopic record. While such shift is clearly

observed in the glacial benthic δ^{13}C values from MIS 30 to MIS 24 (Fig. 2), only a slight amplitude change appears in the glacial benthic δ^{18}O values for the same time interval. The strongest δ^{18}O-enriched value occurs during MIS 22 and MIS 16 (Fig. 2), while the δ^{13}C benthic value does not present low values during MIS 16, for example. Such discrepancies appear clearly in the X–Y isotopic plot (Fig. 3), in which the post-MPT glacial cluster (MIS 24–20) lays far apart from the two end-members mixing line. As long as the most drastic amplitude changes between each MPT glacial periods are not in phase in both isotopic records of the same core, the validity of the hypothesis involving modification in the deep-water masses distribution along the successive MPT glacial interval is doubtful. Meanwhile, such discussion stands for glacial periods only, the role of circulation changes across glacial-interglacial transitions staying undisputed. From our data, we argue that the depletion in the δ^{13}C benthic record of core MD03-2705, observed for the successive MPT glacial interval, could partly be the consequence of a global atmospheric change and its impact on the terrestrial carbon budget. However, more high-latitude benthic records covering the MPT time interval are needed for confirmation.

The 'aridity hypothesis' proposed by Raymo et al. (1997) still needs to be tested for other continents. Indeed, the decrease in carbon isotope values has been observed on a global scale, in each deep ocean basin. For the past 0.80 Ma, a clear link can be observed between global aridification as suggested by atmospheric dust content recovered from the Dome C ice core record (EPICA community members,

2004) and our $\delta^{13}C$ benthic record. For each glacial period of increased dust content in the Antarctic ice, a depletion in the $\delta^{13}C$ benthic record is observed in core MD03-2705 (Fig. 5). Meanwhile, no such global record of atmospheric dust exists for the period prior to 0.8 Ma. Some paleo-records of the East Asian Monsoon extend back one million years. These records are extracted from two red-clay and loess palaeosol sequences observed on the Chinese Loess Plateau (Sun et al., 2006), and are plotted in Figures 5 and 6 along with MD03-2705 records. In the continental Asian records, magnetic susceptibility is believed to represent amplitude and frequency of the eastern Asian summer monsoon. The mean grain size of the Chinese loess, which principally reflects the wind intensity, has been interpreted as a proxy for the intensity of monsoon circulation and aridity in sources area of dust (Xiao et al., 1992). Over the MPT, an increase in the mean grain size is observed for glacial periods MIS 22 and 24, in phase with aridity proxies from the Angola basin (ODP1077) or with wind-strength proxies in the Mauritanian margin (MD03-2705) (Fig. 6). Within the different timescale uncertainties linked to each of these palaeoclimatic records, eastern Asian Monsoon proxies suggest an enhanced winter monsoon activity (coarser grain size) during the MPT, while the summer monsoon is weak (Fig. 5). Such a configuration might have enhanced the aridity over the Asian continent, leading to the same impact over the ocean, i.e. an input from a ^{13}C depleted carbon reservoir into the ocean. The eastern Asian continental aridity (which mainly impacts the Pacific deep waters) reveals the same response when compared to the African continent aridity (which mainly impacts the Atlantic deep waters), and both might have thus triggered similar consequences on the mean deep-water carbon isotopic composition.

Conclusions

Multiproxy analysis of a marine core off the Mauritanian margin has allowed for reconstruction of variations in atmospheric and oceanic dynamics during the last 1.1 Ma. Ti and Quartz contents show past variations in African continental aridity, in agreement with the aeolian terrigenous particle concentration. Within the MPT, an increase of these proxies during consecutive glacial periods (MIS 26, 24 and 22) suggests enhanced aridity over the African continent. These results are consistent with evidence for aridification throughout the African continent, found in the Benguela basin (Marlow et al., 2000) or in the Angola basin (Schefuß et al., 2003). These terrestrial environmental changes correspond to shifts in the deep ocean carbon isotopic composition, with benthic $\delta^{13}C$ minima during the same glacial periods. The proposed link calls for a larger input from the continental ^{13}C depleted carbon reservoir into the ocean as the result of the extension of C_4 vegetation in the arid latitudinal band in Northwest Africa (due to a southern shift of the ITCZ), and facilitated by stronger winds. While the contribution of the West African increased aridity is probably too small to imprint the global deep-water carbon isotopic signature (as also indicated by the phase lag relationship between our terrigenous and $\delta^{13}C$ records), it is likely indicative of a global aridification phenomenon that may have taken place during the MPT.

Similar shifts in the benthic $\delta^{13}C$ have been observed in deep marine cores from different oceans, during the MPT, highlighting the global aspect of such changes. While the $\delta^{18}O$ benthic enrichment expresses the building of bigger continental ice sheets over the high latitudes continents (moving from a '41 ka' climatic cycle world to the '100 ka world'), the $\delta^{13}C$ benthic depletion has been hypothetically linked with global aridity changes (Raymo et al., 1997). On a global scale, we compare our African record with the continental loess record from Asia. For the same time interval, the Asian continent displayed an increased winter monsoon while the summer monsoon remained weak. Such a configuration is likely to have resulted in increased wind strength and aridity over the Asian continent. These two records therefore support Raymo et al.'s (1997) hypothesis of a worldwide input

of carbon from the terrestrial biosphere reservoir into the ocean in order to account for the global deep-water carbon isotopic composition change during the MTP.

In the future, global circulation model runs could help to define the role of atmospheric dynamics during the MPT, and more precisely, test the hypothesis of a shifting ITCZ associated with the cold glacial stages of the MPT (Kageyama et al., 2009).

References

Bertrand, P., Shimmield, G., Martinez, P., Grousset, F., Jorissen, F., Paterne, M., Pujol, C., Bouloubassi, I., Buat-Menard, P., Peypouquet, J.-P., Beaufort, L., Sicre, M.-A., Lallier-Verges, E., Ternois, Y., and other participants of the Sedorqua Program, 1996. The glacial ocean productivity hypothesis: the importance of regional temporal and spatial studies. Marine Geology 130, 1–9.

Bout-Roumazeilles, V., Cortijo, E., Labeyrie, L., Debrabant, P., 1999. Clay mineral evidence of nepheloid layer contribution to the Heinrich layers in the Northwest Atlantic. Palaeogeography, Palaeoclimatology, Palaeoecology 146, 211–228.

Bout-Roumazeilles, V., Nebout, N.C., Peyron, O., Cortijo, E., Landais, A., Masson-Delmotte, V., 2007. Connection between South Mediterranean climate and North African atmospheric circulation during the last 50,000 yr BP North Atlantic cold events. Quaternary Science Reviews 26, 3197–3215.

Broecker, W.S., Peng, T.H., 1982. Tracers in the Sea. Lamont-Doherty Earth Obs, Palisades, NY. 690 pp.

Clark, P.U., Archer, D., Pollard, D., Blum, J.D., Rial, J.A., Brovkin, V., Mix, A., Pisias, N.G., Roy, M., 2006. The middle Pleistocene transition: characteristics, mechanisms, and implications for long-term changes in atmospheric pCO_2. Quaternary Science Reviews 25, 3150–3184.

Curry, W.B., Oppo, D.W., 2005. Glacial water mass geometry and the distribution of $\delta^{13}C$ of $\sum CO_2$ in the Western Atlantic Ocean. Paleoceanography 20, PA1017. doi:10.1029/2004PA001021.

Curry, W.B., Duplessy, J.-C., Labeyrie, L.D., Shackleton, N., 1988. Changes in the distribution of $\delta^{13}C$ of deep water $\sum CO_2$ between the last glaciation and the Holocene. Paleoceanography 3 (3), 317–341.

deGaridel-Thoron, T., Rosenthal, Y., Bassinot, F., Beaufort, L., 2005. Stable sea surface temperatures in the Western Pacific warm pool over the last 1.75 million years. Nature 433, 294–298.

deMenocal, P.B., 1995. Plio-Pleistocene African climate. Science 270, 53–59.

deMenocal, P.B., 2004. African climate change and faunal evolution during the Pliocene–Pleistocene. Earth and Planetary Science Letters 220, 3–24.

deMenocal, P.B., Ortiz, J., Guilderson, T., Adkins, J., Sarnthein, M., Baker, L, Yarusinsky, M., 2000. Abrupt onset and termination of the African Humid Period: rapid climate responses to gradual insolation forcing. Quaternary Science Reviews 17, 395–409.

Duplessy, J.-C., Shackleton, N., 1985. Response of global deep-water circulation to Earth's climatic change 135,000–107,000 years ago. Nature 316 (6028), 500–507.

Duplessy, J.-C., Moyes, J., Pujol, C., 1980. Deep water formation in the North Atlantic Ocean during the last ice age. Nature 286, 479–481.

Duplessy, J.-C., Shackleton, N.J., Matthews, R.K., Prell, W., Ruddiman, W.F., Caralp, M., Hendy, C.H., 1984. 13C record of benthic foraminifera in the last interglacial ocean : Implication for the carbon cycle and the global deep water circulation. Quaternary Research 21, 225–243.

Duplessy, J.-C., Shackleton, N.J., Fairbanks, R.G., Labeyrie, L., Oppo, D., Kallel, N., 1988. Deepwater source variations during the last climatic cycle and their impact on the global deepwater circulation. Paleoceanography 3 (3), 343–360.

Dupont, L., Donner, B., Schneider, R., Wefer, G., 2001. Mid-Pleistocene environmental change in tropical Africa began as early as 1.05 Ma. Geology 29 (3), 195–198.

Epica community members, 2004. Eight glacial cycles from an Antarctic ice core. Nature 429, 623–628.

Flower, B.P., Oppo, D.W., McManus, J.F., Venz, K.A., Hodell, D.A., Cullen, J.L., 2000. North Atlantic intermediate to deep water circulation and chemical stratification during the past 1 Myr. Paleoceanography 15 (4), 388–403.

Hoogakker, B.A., Rohling, E.J., Palmer, M.R., Tyrrell, T., Rothwell, R.G., 2006. Underlying causes for long-term global ocean $\delta^{13}C$ fluctuations over the last 1.20 Myr. Earth and Planetary Science Letters 248, 15–29.

Horng, C.S., Lee, M.Y., Pälike, H., Wei, K.Y., Liang, W.T., Iizuka, Y., Torii, M., 2002. Astronomically calibrated ages for geomagnetic reversals within the Matuyama chron. Earth Planets Space 54, 679–690.

Huelsemann, J., 1966. On the routine analysis of carbonates in unconsolidated sediments. Journal of Sedimentary Petrology 36 (2), 622–625.

Itambi, A.C., von Dobeneck, T., Mulitza, S., Bickert, T., Heslop, D., 2009. Millennial-scale northwest African droughts related to Heinrich events and Dansgaard-Oeschger cycles: Evidence in marine sediments from offshore Senegal. Paleoceanography 24, PA1205. doi:10.1029/2007PA001570.

Jullien, E., Grousset, E.F., Malaizé, B., Duprat, J., Sanchez-Goni, M.F., Eynaud, F., Charlier, K., Schneider, R., Bory, A., Bout, V., Flores, J., 2007. Low latitude 'dusty events' vs high latitude 'Icy Heinrich events'? Research Quarterly 68 (3), 379–386. doi:10.1016/j.yqres.2007.07.007.

Kageyama, M., Mignot, J., Swingedouw, D., Marzin, C., Alkama, R., Marti, O., 2009. Glacial climate sensitivity to different states of the Atlantic Meridional Overturning Circulation : results from the IPSL model. Climate of the Past 5, 551–570.

Kirschvink, J., 1980. The least-squares line and plane and the analysis of paleomagnetic data. Geophysical Journal of the Royal Astronomical Society 62, 699–718.

Kroopnick, P.M., 1985. The distribution of $\delta^{13}C$ of $\sum CO_2$ in the world oceans. Deep-Sea Research Part A 32, 57–84.

Lisiecki, L.E., Raymo, M.E., 2005. A Plio-Pleistocene stack of 57 globally distributed benthic $\delta^{18}O$ records. Paleoceanography 20, PA1003. doi:10.1029/2004PA001071.

Loubere, P., 1991. Deep-sea benthic foraminiferal assemblage response to a surface ocean productivity gradient: a test. Paleoceanography 6 (2), 193–204.

Lutze, G.F., Coulbourn, W.T., 1984. Recent benthic foraminifera from the continental margin of northwest Africa: community structure and distribution. Marine Micropaleontology 8, 361–401.

Mackensen, A., Bickert, T., 1999. Stable carbon isotopes in benthic foraminifera: proxies for deep and bottom water circulation and new production. In: Fisher, G., Wefer, G. (Eds.), Use of Proxies in Paleoceanography: Examples from the South Atlantic Ocean. Springer-Verlag, Berlin Heidelberg, pp. 229–254.

Marlow, J.R., Lange, C.B., Wefer, G., Rosell-Mele, A., 2000. Upwelling intensification as part of the Pliocene–Pleistocene climate transition. Science 290, 2288–2291.

Martinez, P., Bertrand, P., Bouloubassi, I., Bareille, G., Shimmield, G., Vautravers, B., Grousset, F., Guichard, S., Ternois, Y., Sicre, M.-A., 1996. An integrated view of inorganic and organic biogeochemical indicators of palaeoproductivity changes in a coastal upwelling area. Organic Geochemistry 24 (4), 411–420.

Maslin, M., Thomas, E., 2003. Balancing the deglacial global carbon budget: the hydrate factor. Quaternary Science Reviews 1729–1736.

Matsuzaki, K.M.R., Eynaud, F., Malaizé, B., Grousset, F.E., Tisserand, A., Rossignol, L., Charlier, K., Jullien, E., 2011. Paleoceanography of the Mauritanian margin during the last two climatic cycles: from planktonic foraminifera to African climate dynamic. Marine Micropaleontology 79, 67–79. doi:10.1016/j.marmicro.2011.01.004.

Mazaud, A., 2005. User-friendly software for vector analysis of the magnetization of long sediment cores. Geochemistry Geophysics Geosystems 6. doi:10.1029/2005GC001036.

Mulitza, S., Prange, M., Stuut, J.-B., Zabel, M., vonDobeneck, T., Itambi, A., Nizou, J., Schulz, M., Wefer, G., 2008. Sahel megadroughts triggered by glacial slowdowns of Atlantic meridional overturning. Paleoceanography 23, PA4206. doi:10.1029/2008PA001637.

Muller, G., Gatsner, M., 1971. Chemical analysis. Neues Jahrbuch für Mineralogie Monatshefte 10, 466–469.

Oppo, D.W., Lehman, S.J., 1993. Mid-depth circulation of the sub-polar North Atlantic during the Last Glacial Maximum. Science 259, 1148–1152.

Paillard, D., Labeyrie, L., Yiou, P., 1996. Macintosh program makes time-series analysis easy. EOS Transactions, Americain Geophysical Union 77 (39), 379.

Petschick, R., 2000. MacDiff 4.2 Manual. MacDiff. (online). Available from: http://www.geologie.uni-frankfurt.de/Staff/Homepages/Petschick/RainerE.html. (Revised 2001-05-17).

Ravelo, A.C., Andreasen, D.H., Lyle, M., Lyle, A.O., Wara, M., 2004. Regional climate shifts caused by gradual global cooling in the Pliocene epoch. Nature 429, 263–267.

Raymo, M.E., Oppo, D.W., Curry, W., 1997. The mid-Pleistocene climate transition: a deep sea carbon isotopic perspective. Paleoceanography 12 (4), 546–559.

Raymo, M.E., Oppo, D.W., Flower, B.P., Hodell, D.A., McManus, J.F., Venz, K.A., Kleiven, K.F., McIntyre, K., 2004. Stability of North Atlantic water masses in face of pronounced climate variability during the Pleistocene. Paleoceanography 19, PA2008. doi:10.1029/2003PA000921.

Rea, D.K., 1994. The paleoclimatic record provided by eolian deposition in the deep sea: the geologic history of wind. Reviews of Geophysics 32, 159–195.

Richter, T.O., van der Gaast, S., Koster, B., Vaars, A., Gieles, R., de Stigter, H.C., de Haas, H., van Weering, T.C.E., 2006. The Avaatech XRF Core Scanner: technical description and applications to NE Atlantic sediments. In: Rothwell, G. (Ed.), New Techniques in Sediment Core Analysis: Geol. Soc. London Spec. Publ., 267, pp. 39–50.

Sarnthein, M., Winn, K., Jung, S.J.A., Duplessy, J.-C., Labeyrie, L., Erlenkeuser, H., Ganssen, G., 1994. Changes in east Atlantic deepwater circulation over the last 30,000 years: eight time slice reconstructions. Paleoceanography 9 (2), 209–267.

Schefuß, E., Schouten, S., Jansen, F., Damsté, J.S., 2003. African vegetation controlled by tropical sea surface temperatures in the mid-Pleistocene period. Nature 422, 418–421.

Schmiedl, G., Mackensen, A., 1997. Late quaternary paleoproductivity and deep water circulation in the eastern South Atlantic Ocean: evidence from benthic foraminifera. Paleogeography, Paleoclimatology, Paleoecology 130, 43–80.

Shackleton, N.J., Opdyke, N.D., 1973. Oxygen isotope and palaeomagnetic stratigraphy of equatorial Pacific core V28-238: oxygen isotope temperatues and ice volumes on a 100 kyrs and 1000 kyrs scale. Journal of Quaternary Research 3 (1), 39–54.

Shackleton, N.J., Berger, A., Peltier, W.R., 1990. An alternative astronomical calibration of the lower Pleistocene timescale based on ODP Site 677. Transactions of the Royal Society Edinburgh: Earth Sciences 81, 251–261.

Shackleton, N., Hall, M., Vincent, E., 2000. Phase relationship between millennial-scale events 64,000–24,000 years ago. Paleoceanography 15 (6), 565–569.

Singer, B.S., Brown, L.L., 2002. The Santa Rosa event: 40Ar/39Ar and paleomagnetic results from the Valles rhyolite near Jaramillo Creek, Jemez Mountains, New Mexico. Earth and Planetary Science Letters 197, 51–64.

Singer, B.S., Hoffman, K.A., Pringle, M.S., Chauvin, A., Coe, R.S., 1999. Dating transitionally magnetized lavas of the late Matuyama Chron: toward a new 40Ar/39Ar timescale of reversals and events. Journal of Geophysical Research 104, 679–693.

Sun, Y., Clemens, S.C., An, Z., Yu, Z., 2006. Astronomical timesclae and palaeoclimatic implication of stacked 3.6-Myr monsoon records from the Chinese Loess Plateau. Quaternary Science Reviews 25, 33–48. doi:10.1016/j.quascirev.2005.07.005.

Tisserand, A., Malaizé, B., Jullien, E., Zaragosi, S., Charlier, K., Grousset, F., 2009. African monsoon enhancement during a cold stage, Marine Isotopic Stage 6.5 (MIS6.5), 170 kyr ago. Paleoceanography. doi:10.1029/2008 PA001630.

Tjallingii, R., Claussen, M., Stuut, J.-B., Fohlmeister, J., Jahn, A., Bickert, T., Lamy, F., Röhl, U., 2008. Coherent high-and low-latitude control of the northwest African hydrological balance. Nature Geosciences 1. doi:10.1038/ngeo289.

Vidal, L., Schneider, R.R., Marchal, O., Bickert, T., Stocker, T.F., Wefer, G., 1999. Link between the north and south Atlantic during the Heinrich events of the last glacial period. Climate Dynamics 15, 909–919.

Weeks, R., Laj, C., Endignoux, L., Fuller, M., Roberts, A., Manganne, R., Blanchard, E., Goree, W., 1993. Improvements in long-core measurement techniques: applications in palaeomagnetism and palaeoceanography. Geophysical Journal International 114, 651–662.

Xiao, J., Hongbo, Z., Zhao, H., 1992. Variation of winter monsoon intensity on the Loess plateau, Central China during the Last 130,000 years : evidence from grain size distribution. Quaternary Research 31 (1), 13–19.